processes

MDPI

Article

A Study on the Evolution of Coal Seam Stress and Permeability During Coal Mining and Its Application Effects: A Case Study of T Coal Mine

Jie Gao [1], Lihua Wang [1,*], Zhenhua Hu [2,*], Wei Zhao [3], Zhengyu Yang [4], Hongxing Zhou [2], Dong Liu [5] and Tao Wang [3]

[1] State Key Laboratory for Fine Exploration and Intelligent Development of Coal Resources, School of Mines, University of Mining and Technology, Xuzhou 221116, China; gaojie@cumt.edu.cn
[2] School of Safety Engineering, China University of Mining and Technology, Xuzhou 221116, China; zhou12510@126.com
[3] Chensilou Coal Mine, Henan Longyu Energy Co., Ltd., Yongcheng 476600, China; lb21120037@cumt.edu.cn (W.Z.); wtxx1986@sina.com (T.W.)
[4] Science and Technology Innovation Center, Henan Energy Group Co., Ltd., Zhengzhou 450053, China; yangzhengyu@hnecgc.com.cn
[5] Institute of Chemical Engineering and Design, Henan Energy Group Research Institute Ltd., Zhengzhou 450046, China; liudong860614@126.com
* Correspondence: 4449@cumt.edu.cn (L.W.); h17854297791@163.com (Z.H.)

Abstract

Background: The pressure reduction range in traditional protective coal mining is often set conservatively, resulting in diminished actual pressure reduction effects near the mining boundary. Therefore, analyzing the stress and permeability evolution patterns at the mining boundary is particularly essential. Method: A three-dimensional numerical model was established according to the mining conditions of the 864 working face in T Mine to study the stress evolution, fissure development, and permeability evolution of the coal and rock mass overlying the protective seam mining, especially those near the mining boundary. Results: The overlying coal and surrounding rock mass near the mining boundary are in the state of increasing vertical stress and decreasing horizontal stress, and under this mechanical path of "increasing axial pressure and decreasing peripheral pressure", the coal mass is damaged and destroyed, fissures are developed, and the permeability is increased; as a result, the coal and surrounding rock mass near the mining boundary mainly produce vertical longitudinal fissures, and the permeability can be increased 900 times compared with that of the overlying coal and surrounding rock mass in the mining boundary. After ground drilling and enhanced depressurization, the measured maximum gas content of the coal mass at the strike boundary is 3.25 m^3/t, and the measured maximum gas content of the coal mass at the inclination boundary is 2.63 m^3/t. Conclusions: After mining the protective layer, the permeability enhancement effect diminishes from the center toward the sides, yet remains sufficient to eliminate the risk of gas outbursts. This validates the importance of verifying permeability enhancement effects at coal seam boundaries.

Keywords: mining of protective seam; numerical simulation; permeability; scope of protection; pressure relief effect

Academic Editor: Qingbang Meng

Received: 9 January 2026
Revised: 28 January 2026
Accepted: 2 February 2026
Published: 4 February 2026

1. Introduction

As mining depths continue to increase, geological structures become increasingly complex, with gas pressure and permeability issues posing significant constraints to coal mining safety [1,2].

Protective layer mining serves as an effective method for pressure relief [3], Following protective layer mining, roof pressure is released, and the resulting fractures facilitate the continuous conversion of coalbed methane from adsorbed to free gas [4,5]. Therefore, investigating the evolution patterns of stress and fracture fields in the roof coal–rock mass during protective coal seam mining provides significant guidance and reference value for implementing effective measures at the mining site.

The mining of protective coal seams disrupts the original stress equilibrium state, initiating a process of stress redistribution and inducing fractures [6,7]. Numerous scholars have investigated the stress distribution and deformation characteristics of the roof in goaf areas, establishing a fundamental understanding of the basic patterns of stress distribution during the mining process [8]. Under actual coal seam conditions, the stress of the coal mass is complex and changeable; it is often affected by mining and undergoes a process of decreasing horizontal stress and increasing vertical stress [9,10]. With the increasing stress concentration of coal and surrounding rock mass in the working face, the pressure relief effect gradually becomes significant [11,12]. In view of this, Jia [13,14] analyzed the influence of the trend and tendency of the overlying coal mass on stress and pointed out that the stress is mainly concentrated in the Z direction and has little influence on the horizontal stress. In addition, Yin Wei [15] established a correlation model between stress evolution and fracture depth by studying the stress evolution and fracture distribution of the overlying coal and surrounding rock mass. Cheng et al. [16] found that mining of the protective seam will produce a dynamic effect, resulting in the plastic failure of the nearby coal rock seams under the influence of dynamics, and a large number of separation and vertical fractures will appear. After being affected by mining, the protected seam undergoes pressure relief and expansion deformation, accompanied by stress reduction and increased permeability of the surrounding rock, which results in the formation of interconnected longitudinal and transverse fractures [17]. Xie et al. [18] simulated the deformation and pressure relief effect of the overlying coal rock and proposed that the pressure relief of the protective seam can be determined by analyzing the changes in stress and permeability of the protected seam. Recent studies have further advanced the understanding of pressure relief mining and permeability enhancement in protected seams, including spatiotemporal permeability evolution associated with key-strata fracture and field-oriented evaluation of gas extraction effectiveness [19–21]. Meanwhile, experimental and modeling efforts have highlighted the strong dependence of coal permeability on mining disturbance paths, cyclic loading–unloading histories, and gas drainage conditions [22,23]. In addition, mining-induced fracture network reconstruction and anisotropic permeability evaluation have received increasing attention, underscoring the role of evolving fracture connectivity in permeability enhancement [24,25].

Existing studies on protective seam mining can be broadly classified into three dominant lines of research. First, continuum-based numerical simulations focus on stress redistribution and delineation of pressure relief zones, which are effective for capturing macroscopic stress evolution but often provide limited information on fracture connectivity and preferential transport pathways. Second, although analysis methods based on discontinuous media (such as discrete element modeling) can describe fracture initiation and geometric morphology, they are often confined to local scales and struggle to establish consistent links with permeability enhancement at the engineering scale. Third, permeability evolution models and coupled rheological frameworks aim to link mining-induced stress changes with transport characteristics, yet they often simplify boundary heterogeneity and fail to explicitly quantify boundary-specific stress paths and their impact on permeability enhancement. Particularly in boundary regions, studies typically adopt conservative treatments, resulting in insufficient systematic quantitative correlations between boundary stress evolution, fracture development, and permeability improvement. To address this gap, this study integrates three-dimensional boundary stress path characterization, fracture morphology interpretation, and stress-driven permeability evolution. The predicted decompression effects were validated using field gas content data.

The main contributions of this study are threefold: (1) quantitatively characterize the three-dimensional stress evolution paths in the boundary zones of protective seam mining, where vertical stress concentration and horizontal stress relief coexist and are often underestimated in conventional analyses; (2) establish a consistent linkage between stress evolution, fracture development patterns in boundary regions, and the spatial evolution of permeability enhancement, thereby connecting mechanical responses to permeability changes in a unified framework; (3) validate the simulation-based findings using field gas extraction data, which improves the engineering relevance of the proposed boundary zone assessment.

2. Materials and Methods

The numerical simulation was performed using the stratigraphy of the 864 mining area of T coal mine, and Rhino 6.0 (Shanghai, China) software was used for modeling. Considering the boundary effect and the actual situation of the mining area, the mechanical parameters of each stratum are shown in Table 1, and the model is set to be 600 m long in the direction of strike, 400 m in the direction of inclination, and 179.5 m in height; the angle of inclination of the coal and rock seam is 10°. The mining face is located in the 8_2 coal seam, which is located 37 m below the protected 7 coal seam, the mining height of the coal seam is 2.5 m, and the coal thickness of the protected 7 coal seam is 2.5 m. The model boundary is imposed and the mining method is shown in Figure 1.

Table 1. Mechanical parameters of each layer of coal and rock mass.

Batch Number	Lithology	Density/kg/m^3	Bulk Modulus/GPa	Shear Modulus/GPa	Cohesion/MPa	Angle of Internal Friction/°	Tensile Strength/MPa
1	limestone	2690	14	11	2.42	36	2.93
2	shale	2590	12	9	1.82	33	1.96
3	7 coal seam	1300	1.5	1.2	1	18	1
4	siltstone	2560	14	9	1.69	33	1.86
5	8_2 coal seam	1300	1.5	1.2	1	18	1

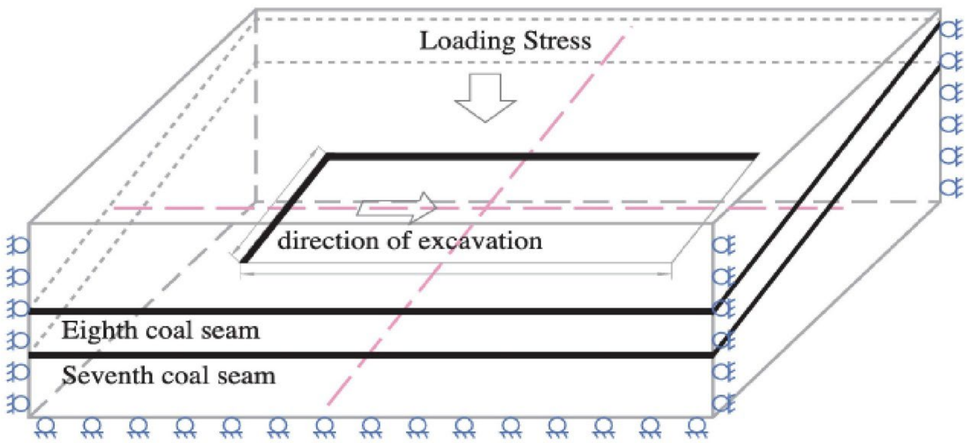

Figure 1. Model boundary conditions and numerical models.

The Mohr–Coulomb Model (MCM) was selected due to its widespread application in coal seam and surrounding rock engineering to describe stress redistribution, plastic deformation, and failure behavior induced by underground mining [26,27]. This study focuses on the macroscopic response of coal seams and surrounding rock, including stress evolution, pressure release range, and permeability enhancement. The MCM is a continuum, elastic–perfectly plastic representation and therefore does not explicitly simulate fracture initiation, propagation, and connectivity, nor does it inherently capture strain softening and progressive damage. Therefore, fracture characteristics are examined using a discrete element simulation to support the interpretation of boundary fracture evolution. To synthesize the actual situation of the stratum, the model adopts zero displacement constraints for the left, right, front, back, and bottom; the upper part is the free boundary. Moreover, 10 MPa vertical stress and 10 MPa gradient stress is applied to the model in the X and Y directions, and the gravitational acceleration is set to 9.8 m/s^2. The numerical calculation model is shown in Figure 2. A vertical stress of 10 MPa is applied to simulate the gravitational stress generated by the overlying strata at the coal seam's burial depth, consistent with the in situ stress conditions at T Coal Mine. Horizontal stresses in the X and Y directions are applied using a gradient distribution to simulate the regional tectonic stress field and its spatial variations. These stresses are defined as initial stress conditions to establish the pre-mining equilibrium state for the model, rather than as external loads during the mining process.

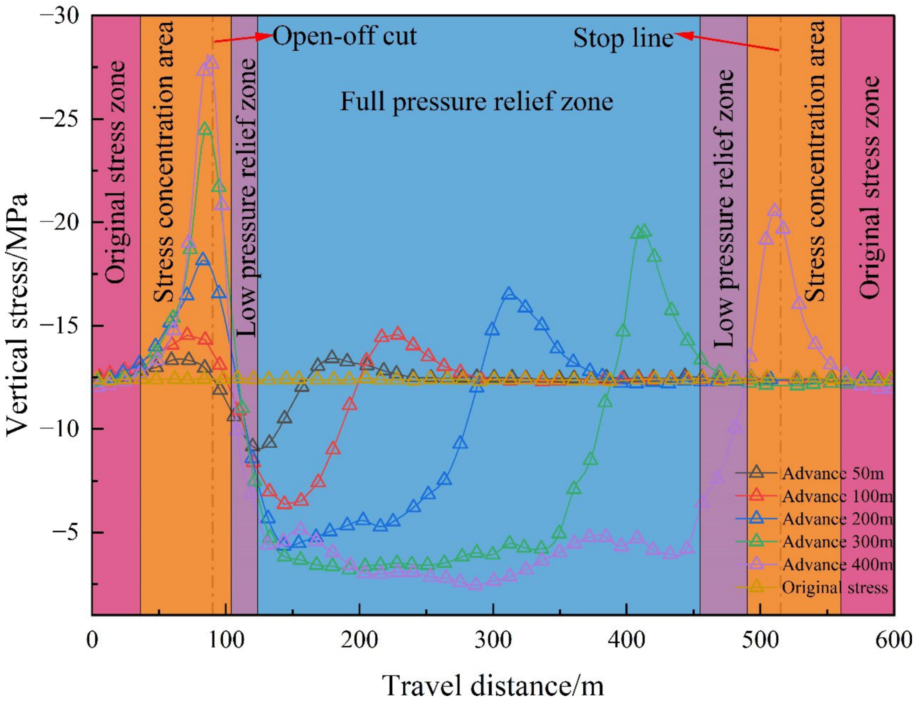

Figure 2. Vertical stress variation curve in strike direction.

The total number of cells in the model mesh is 6.75×10^5. The model is first brought to a pre-mining static equilibrium under the imposed initial stress field. After each excavation step, the calculation is iterated to a quasi-static equilibrium until the ratio of the global unbalanced force to the global applied force is less than or equal to 1×10^{-5}. To assess the impact of modulus uncertainty, the elastic modulus is varied within a ±5% range around its baseline value while maintaining the initial stress field and all numerical settings. The percentage reduction in horizontal stress in the strike direction fluctuates between 88.2% and 89.6%. The corresponding reduction in dip–slope horizontal stress ranges from 78.9% to 80.6%. Concurrently, the maximum permeability enhancement factor varies between

870 and 930. Overall, the key indicators exhibit limited fluctuation within the tested elastic modulus range.

3. Results

3.1. Vertical Stress Evolution Law

Prior to the mining of the protective layer, the coal–rock mass remained in a stable equilibrium state under three-dimensional stress. As the protective layer was mined, the goaf gradually formed, disrupting the original stress balance. Under the influence of self-weight stress, the overlying coal–rock mass underwent failure and fissure development, leading to downward movement. Simultaneously, the floor of the goaf experienced expansion deformation, resulting in floor heave. To investigate stress variations and distribution patterns in the overlying coal–rock mass under different longwall advance conditions, two monitoring lines were established in the protected roof. These lines tracked the evolution of normal stresses along strike and dip directions at different advance distances. By analyzing stress variation patterns perpendicular to strike and dip in the coal seam roof under varying advance distances, the stress variation curves depicted in Figures 2 and 3 were generated.

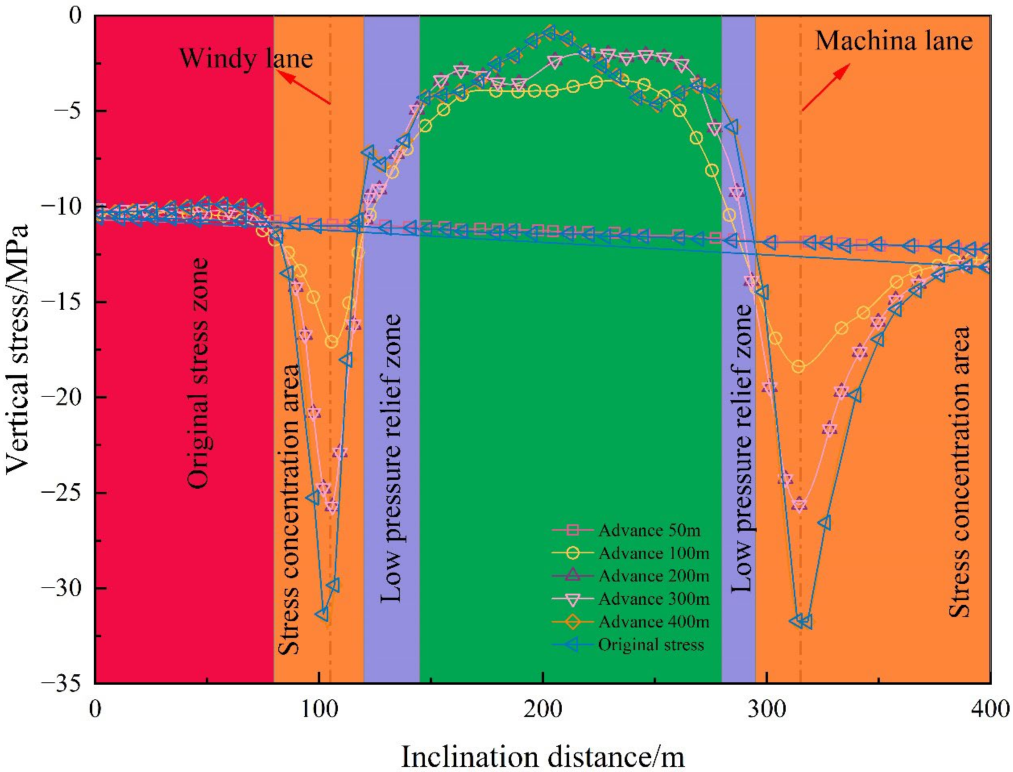

Figure 3. Vertical stress variation curve in inclination direction.

As the working face advanced 400 m along the strike direction, the coal–rock mass sequentially entered into the following stress zones in both strike and incline directions: the original rock stress zone, the stress concentration zone, the low-pressure unloading zone, and the fully decompressed zone. Significant stress concentration formed near the cutting eye and stop line, corresponding to the protected layer location. Vertical stress at the cutting eye increased from an initial 11.3 MPa to 27.5 MPa, while at the stop line it rose from 10.74 MPa to 20.0 MPa. The vertical stress in the coal body ahead of the working face first reached a peak, then rapidly decayed, and ultimately returned to the original rock stress level. The area above the goaf constituted a fully pressure-relieved zone, with its unloading range gradually expanding with the scale of the goaf. As mining progressed, the degree of unloading at the same location continuously deepened.

The vertical stress variation curve in the dip direction indicated that the unloading reached its maximum when the working face advanced 400 m. Due to the shallow burial depth of the ventilation drift, its original rock vertical stress was lower than that of the haulage drift. After face extraction, stress concentration zones formed near both the ventilation and haulage drifts. Specifically, stress in the coal body outside the ventilation drift increased from 10.5 MPa to 30.8 MPa, while stress in the coal body outside the haulage drift rose from 11.7 MPa to 31.3 MPa.

3.2. X, Y Horizontal Stress Evolution Law

Existing studies on the pressure relief effect of protective seam mining mainly focus on variations in vertical stress, while relatively few have investigated the evolution of horizontal stress and its influence on pressure relief. Therefore, two monitoring lines were arranged on the roof of the protected seam to record the numerical evolution of the lateral stress components in the Y direction (SYY) and the X direction (SXX) along the inclination of the coal seam roof as the working face advanced different distances.

The horizontal stress distribution along the strike direction is shown in Figure 4. After protective seam mining, pressure relief zones formed in front of the open-off cut and near the working face, where the horizontal stress decreased significantly and fell below the original in situ stress. When the working face advanced to the stopping line, the pressure relief effect reached its maximum: the Y-direction lateral stress component SYY decreased from an initial value of 8.28 MPa to 0.92 MPa, corresponding to a pressure relief rate of 88.9%. Meanwhile, the overall stress distribution curve changed from a "V"-shaped to a "U"-shaped pattern.

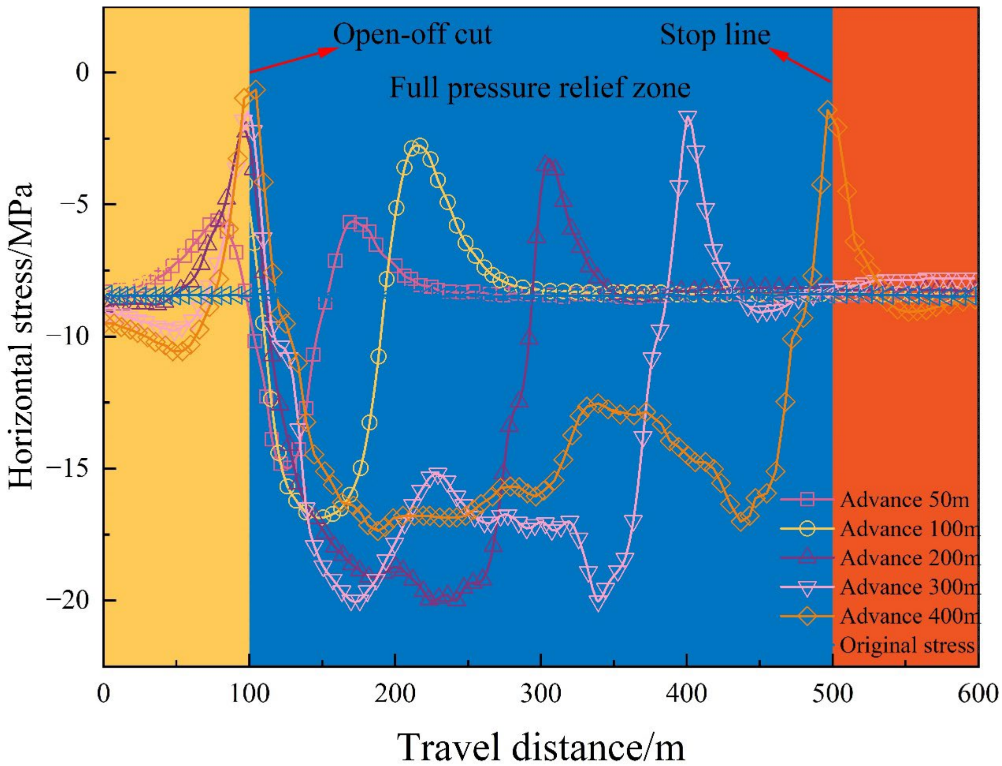

Figure 4. SYY stress distribution curve of strike direction.

Due to differences in burial depth, Figure 5 shows that horizontal stress exhibits a gradient distribution along the inclination direction, with the X-direction lateral stress component SXX gradually increasing from the wind tunnel to the machine tunnel. As the protected seam bent and subsided, the horizontal stress in the coal seam floor increased. In contrast, obvious pressure relief zones developed at the wind tunnel and machine tunnel, where the horizontal stress decreased. At the same time, the pressure relief range of the coal seam gradually expanded with mining advancement, and the degree of pressure relief in the machine tunnel was greater than that in the wind tunnel. Compared to machine roadways, ventilation roadways are shallower in burial depth. As indicated by the original stress distribution, ventilation roadways exhibit lower initial stress levels. Consequently, after the working face was mined, the pressure relief effect in ventilation roadways was more effective. When the working face advanced to the stopping line, the pressure relief range reached its maximum, with SXX decreasing from an initial 8.28 MPa to 1.68 MPa, corresponding to a pressure relief rate of 79.7%.

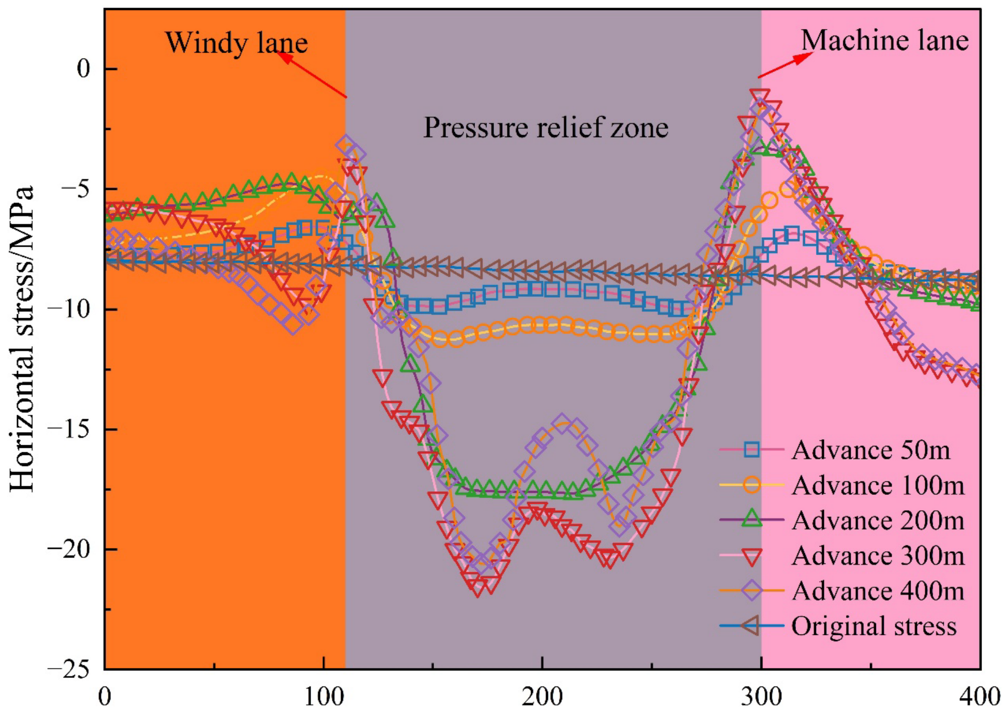

Figure 5. SYY stress distribution curve of inclination direction.

Analysis of the evolution of vertical and horizontal stresses indicates that, after protective seam mining, the vertical stress in the protected seam increased in the coal mass corresponding to the open-off cut, the area in front of the working face, the machine roadway, and the wind tunnel, forming distinct stress concentration zones. In contrast, the horizontal stress in the protected seam decreased at these corresponding locations, which act as pressure-relief zones. The stress relief area in the X direction was mainly distributed in the coal mass associated with the machine roadway and wind tunnel, whereas the stress-relief area in the Y direction was primarily concentrated in the coal mass in front of the open-off cut and the working face. Overall, protective seam extraction induced a characteristic stress evolution pattern in the protected coal mass, characterized by an increase in vertical stress and a decrease in horizontal stress.

3.3. Characterization of Fracture Distribution

After protective seam mining, the stress state of the overlying strata above the goaf was significantly altered. Along the boundary of the 864 goaf, a characteristic stress evolution pattern is observed, characterized by increased vertical stress and reduced horizontal stress. During stress readjustment toward a new equilibrium, the coal seam underwent different degrees of subsidence toward the mined-out void. UDEC, two-dimensional discrete element method-based software (https://www.itasca.se/en/software/udec, accessed on

8 January 2026), is well suited for analyzing the evolution of overburden fractures and was therefore employed to simulate the development of overburden fissures. Under mining-induced stress redistribution, the coal and rock masses are subjected to both tensile and compressive stresses: tensile stress promotes fracture initiation and propagation, whereas compressive stress leads to the closure of pre-existing fractures. Following protective seam extraction, staggered horizontal fractures, interlayer fractures, and vertically penetrating fractures are formed.

Figures 6 and 7 illustrate the evolution of overburden fractures along the strike and inclination directions when the working face advances to the stopping line. The protected seam bends and subsides, forming a distinct fracture zone, and the fracture distribution is consistent with the three-dimensional stress evolution pattern. In the central fracture zone, vertical stress unloading is most pronounced, causing tensile separation along the contact surfaces between adjacent rock layers and resulting in the development of interlayer horizontal fractures accompanied by a small number of vertical fractures. In contrast, in the overlying coal seam areas corresponding to the front of the working face and the open-off cut, a large number of vertical fractures develop within the pressure relief zones due to the reduction in horizontal stress. These fractures are further expanded by continued horizontal stress unloading, producing an inverted trapezoidal fracture distribution characterized by a wider upper part and a narrower lower part.

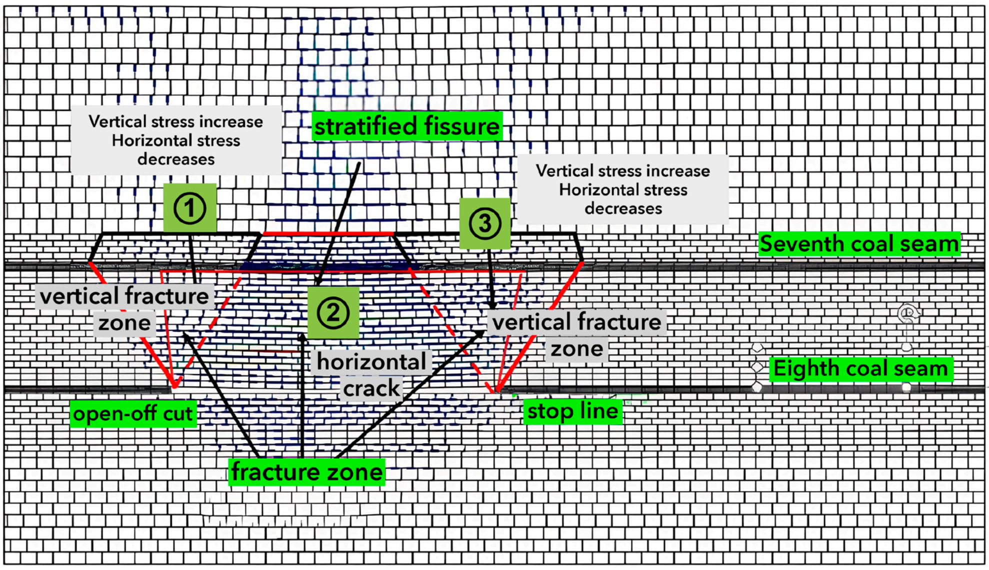

Figure 6. Volution cloud diagram of overburden fractures in direction of strike. Notes: ①, ③ vertical fracture zone; ② stratified fissure.

After protective seam mining, overburden fractures developed predominantly along the inclination direction. The horizontal stress in the coal strata near the air roadway and the machine roadway was significantly reduced, resulting in more effective pressure relief. In areas ① and ③, a large number of vertically penetrating fractures were generated, which are more pronounced than those observed in the strike direction. Under the continued influence of horizontal stress reduction, the fracture pressure relief zone expanded into a larger inverted trapezoidal shape, providing favorable pathways for gas migration and extraction.

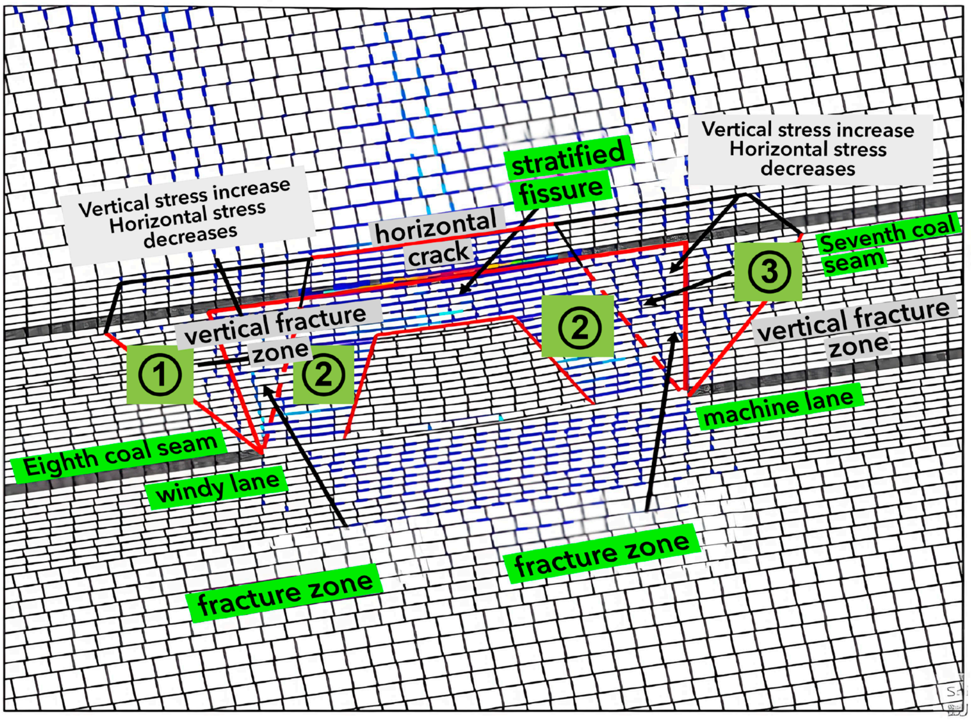

Figure 7. Trend direction overburden fracture evolution cloud map. Notes: ①, ③ vertical fracture zone; ② horizontal fissure.

3.4. Fracture and Stress Evolution Rules

After protective seam exploitation, the fissure distribution was closely associated with the stress and deformation state of the coal–rock mass. The boundary of the overlying strata underwent horizontal stress reduction and vertical stress increase. Under horizontal stress unloading, the fissure zone continuously expanded, leading to the formation of numerous vertical fissures that gradually interconnect [19]. Only shear damage was produced in the coal rock under fixed-envelope plus axial pressure conditions in the laboratory [20]. The peak point was 32.33 MPa for fixed-enclosure pressure and 22.95 MPa for unloaded enclosure pressure when the initial enclosure pressure was 10 MPa. The peak point differential stress of coal samples under the unloaded-enclosure plus axial pressure path decreased by 29.0% compared to that of the fixed-enclosure plus axial pressure path. The process of unloading the perimeter pressure can make the peak destructive strength of the coal mass decrease dramatically, so unloading of the perimeter pressure can help to reduce the difficulty in destroying the coal body and expand the scope of coal body destruction [20]. After protective seam exploitation, the overlying coal rock body boundaries are more likely to be damaged by the fissure.

3.5. Fracture and Permeability Variations

The variation in the stress state of the coal mass can cause damage to it, and the cracks produced by this damage can increase the permeability of the coal mass to varying degrees [20]. To explore the effect of different paths of coal damage permeability increase, as shown in Figure 8, the minimum permeability measured under the two paths was 0.00021 mD and 0.00016 mD, the initial permeability was 0.022 mD and 0.028 mD, and the two paths under the measured permeability reached 1.655 mD and 9.632 mD, compared with the initial conditions of permeability. The multiplicity of the sudden increase reached 75.2 times and 344 times, respectively. The greater permeability of the damaged media under the unloaded-containment plus axial path compared to under the fixed-containment plus axial path suggests that the damaged coals under the unloaded containment condition are able to obtain better penetration enhancement. Due to the effect of horizontal depressurization, a large number of vertical fissures can be developed at the mining boundary of the overlying coal and rock body, and the fissures are connected with each other, forming a gas transportation network. This increases the permeability of the coal and rock, and the effect of penetration enhancement can be improved.

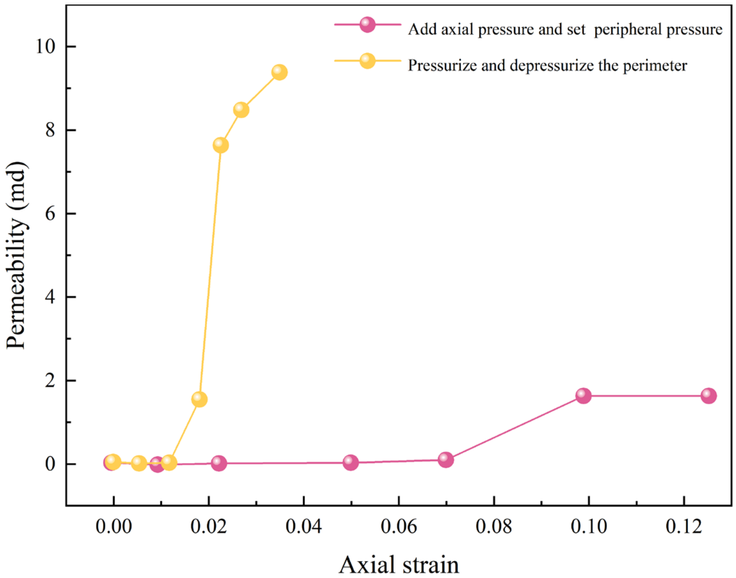

Figure 8. Coal permeability test results under different mechanical paths at initial confining pressure of 10 MPa.

Figure 9 indicates that at an initial confining pressure of 10 MPa, the peak stress under the constant confining pressure path reaches 32.33 MPa, while the peak under the decompression path is 22.95 MPa. The peak stress difference in the decompression plus axial pressure path is reduced by 29.0% compared to the constant confining pressure plus axial pressure path. The unloading process significantly reduces the peak failure strength of the coal body, meaning it facilitates easier failure initiation and expands the failure zone. Consequently, after protective layer mining, the boundary coal body within the overlying coal-=–rock mass becomes more susceptible to failure and fissure formation. Combining Figures 8 and 9 reveals that during protective layer mining, when deviatoric stress reaches 9.4 MPa, axial strain reaches 0.01–0.02, at which point permeability increases, indicating crack initiation. When deviatoric stress reaches 19.6 MPa, permeability surges within the axial strain range of 0.19–0.022, indicating the fastest crack development rate at this stage.

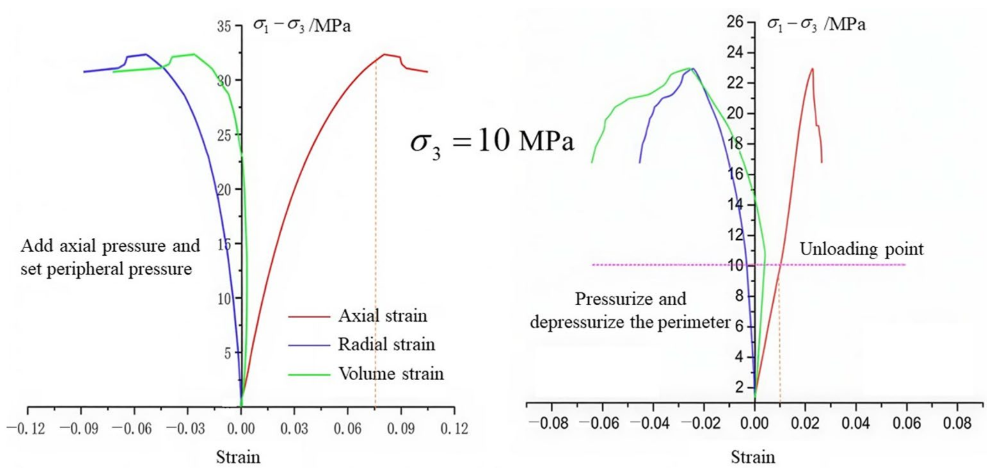

Figure 9. Shear stress–strain curves of coal samples under two mechanical pathways.

4. Discussion

4.1. Relationship Between Coal Rock Permeability and Stress Variations

When mining the protective seam, the overlying coal and surrounding rock mass are affected by horizontal stress, resulting in the coal and surrounding rock mass being damaged, and a large number of vertical cracks are generated at the boundary. An accurate understanding of the evolution rule of permeability and three-dimensional stress in the process of damaging and destroying coal and surrounding rock mass has certain guiding significance for the examination of the effect of pressure relief and gas extraction after mining of the protective seam.

There are three types of stress–permeability relationships: the elastic phase, the inelastic–plastic damage phase, and the residual strength phase. Permeability varies greatly when the coal and surrounding rock mass are in different stages. In this case, after the damage expansion occurred in the coal and surrounding rock mass, the difference between the permeability at the end of the inelastic–plastic damage stage and the residual strength stage was small, and both were at a high level, meaning that they are categorized into the same permeability evolution model.

The evolution model of coal–rock permeability under isotropic stress variations throughout the stress–strain process comprises elastic and inelastic stages, respectively, described by Equations (1) and (2) [28,29]:

$$\frac{k}{k_0} = \left(1 + \frac{\Delta\sigma_x + \Delta\sigma_y + \Delta\sigma_z}{E\Psi_0}\right)^3 \tag{1}$$

$$\frac{k}{k_0} = \left(\frac{1 - \Psi_0 - \varepsilon_{VG}}{(1 - \Psi_0)\dfrac{\Delta\sigma_x + \Delta\sigma_y + \Delta\sigma_z}{E}}\right)^2 \left(1 + \frac{\Delta\sigma_x + \Delta\sigma_y + \Delta\sigma_z}{E\Psi_0}\right)^3 \tag{2}$$

In the above formula: k—coal rock permeability, mD;

k_0—initial permeability of coal rock, mD;

E—modulus of elasticity, MPa;

Ψ_0—initial porosity ratio;

ε_{VG}—coal rock volumetric strain at damage amplification threshold G;

$\Delta\sigma_x$, $\Delta\sigma_y$, $\Delta\sigma_z$—incremental stress in each direction, MPa.

From Equations (1) and (2), it can be seen that, in addition to the effect of stress variation, the permeability of coal rock is related to the porosity and elastic modulus of the coal seam. In order to obtain the relevant data, we obtained coal samples from different locations near coal seam 7 in the coal mine and carried out experimental measurements. The results of the determination of the porosity of the coal samples are shown in Table 2.

Table 2. Determination results of porosity of 7 coal seam in T Coal Mine.

Sequence Number	Sampling Spot	Porosity %	Mean Value %
1	86 Auxiliary return air 1#	6.4	6.9
2	86 Auxiliary return air 2#	7.1	
3	86 Auxiliary return air 3#	6.8	
4	86 Rail downhill No. 3 Train yard G14	7.3	

From the above table, it can be seen that the average value of porosity of the coal samples obtained from different locations near the 7 coal seam of T Mine is 6.9%, and the elastic modulus of the coal seam is 2.16 Gpa. By substituting the porosity and elastic modulus into (1) and (2), a model for the evolution of permeability in 7 coal seam at T Coal Mine during protective mining can be derived, as shown in Equations (3) and (4).

$$\frac{k}{k_0} = \left(1 + \frac{\Delta\sigma_x + \Delta\sigma_y + \Delta\sigma_z}{1.49 \times 10^8}\right)^3 \tag{3}$$

$$\frac{k}{k_0} = \left(\frac{0.93 - \varepsilon_{VG}}{0.93 \times \frac{\Delta\sigma_x + \Delta\sigma_y + \Delta\sigma_z}{2.16 \times 10^9}}\right)^2 \left(1 + \frac{\Delta\sigma_x + \Delta\sigma_y + \Delta\sigma_z}{1.49 \times 10^8}\right)^3 \tag{4}$$

Equations (3) and (4) above represent permeability models for the protective 7 coal seam that evolve with three-dimensional stress variations during mining operations. Equation (3) describes the elastic stage, while Equation (4) characterizes the inelastic stage. This model reflects the evolution and distribution characteristics of permeability based on stress values monitored during numerical simulation.

4.2. Characterization of the Permeability Distribution of the Protected Coal Seam

Using the evolution model of permeability related to three-dimensional stress during the full stress–strain process in coal rock bodies, the 3D geometric model in FLAC3D 7.0 (Zhejiang, China) was reconstructed in COMSOL Multiphysics 6.2 (Shanghai, China) software, and the permeability evolution control equations were written into COMSOL Multiphysics for simulation and solution.

In order to further study the distribution characteristics of the permeability of the protected seam, the permeability distribution plan was extracted and analyzed when the protected seam was mined for 400 m.

With further mining of the protective seam, the coal mass in the elastic stage of permeability evolution enters the inelastic damage stage, the volumetric stress is reduced, the cracks within the coal mass merge together, and the permeability performance is substantially improved. As shown in Figure 10, the red area is sufficiently unpressurized, and the permeability of the middle part of the protected layer is greatly increased after mining of the protected seam is completed. The permeability of the mining boundary is as high as 2.6×10^3 at the initial ratio, and the area of the zone in which permeability increases reaches the maximum. After mining the working face of the protected seam, the permeability of the protected seam is significantly increased in a wide range of areas, and the permeability gradually decreases from the middle of the coal seam to the outside. The permeability evolution area can be divided into an area of greatly increasing permeability, increasing permeability, decreasing permeability, and original permeability; the whole area is distributed according to the characteristics of permeability from high to low in order.

According to the fissure development and permeability change of the boundary of the overlying coal and surrounding rock mass, we set up a measurement line along the direction of the trend of the protected seam at a position of 200 m, calculated the initial ratio of the permeability of the mining boundary, and imported the monitoring data into origin to draw the permeability evolution curve shown in Figure 11. $k/k_0 < 1$ means that permeability decreases, and $k/k_0 > 1$ means that permeability increases. Therefore, under the influence of horizontal stress unloading, the permeability ratio of the open-off cut and the stop line corresponding to the position of the protected seam can be up to 900 times, the permeability performance improves dramatically, higher than in the initial state, and the coal mass is sufficiently unpressurized.

It should be noted that treating permeability as isotropic may underestimate the increase along the dominant connected fracture direction, where preferential flow pathways form, but overestimate the increase in directions with limited connectivity perpendicular to the main fracture set. Neglecting explicit coupling with gas flow may overestimate permeability at later drainage stages because pore pressure decline increases effective stress and can partially close fractures, although matrix shrinkage and irreversible damage may offset this effect to some extent.

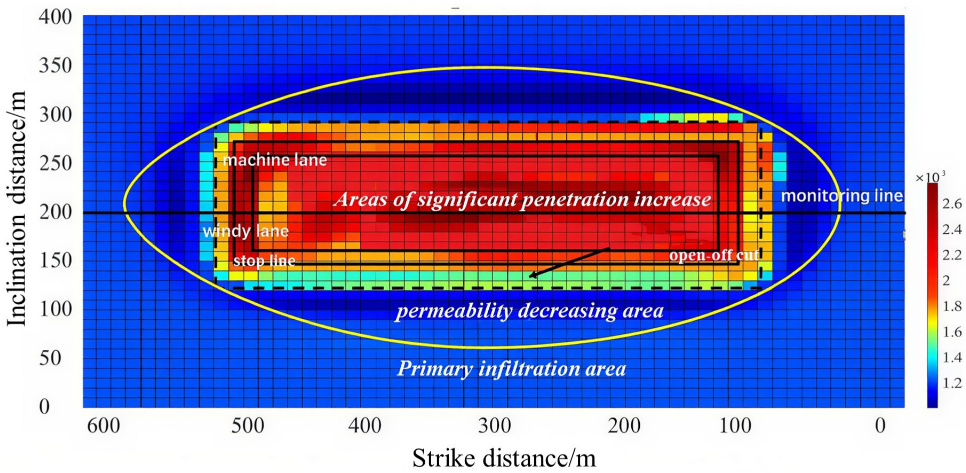

Figure 10. A floor map of the permeability distribution of the protective layer.

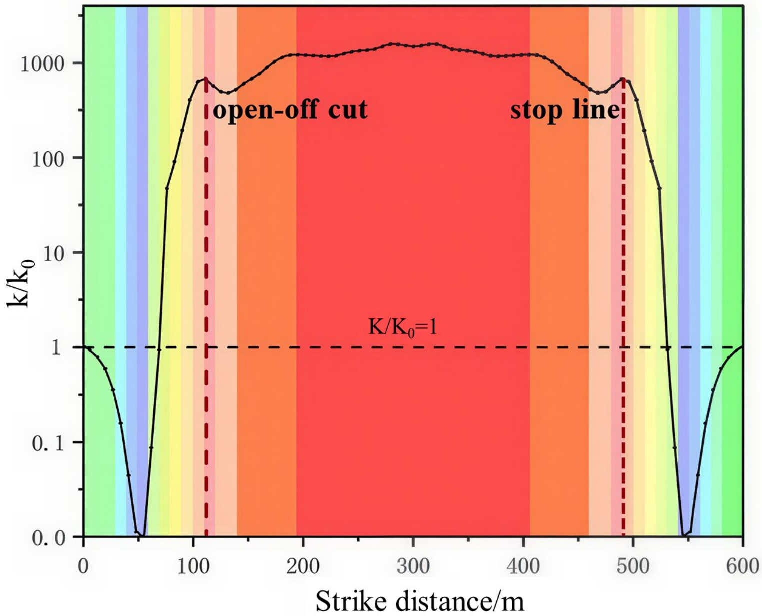

Figure 11. Penetration rate distribution curve.

4.3. Research on the Effect of Pressure Relief Gas Extraction

During the mining process of the working face of the protective layer, numerical simulation was used to change the rule of three-dimensional stress and permeability of the overlying coal and surrounding rock mass and to verify the effect of pressure unloading of the protective seam mining. About seven days after the completion of mining, surface drilling and water pumping were carried out. A series of screening boreholes, designated Z1–Z5 and Q1–Q7, were arranged at the site. The boreholes were deployed from the center of the working face along both the strike and inclination directions. The distribution curve of gas content direction and tendency was drawn.

The distribution of gas content in the strike direction is shown in Figure 12. The maximum gas content measured by the strike boundary survey borehole was 3.25 m^3/t under the intensified pumping of surface drilling, which is smaller than the critical value for determining the risk of protrusion as stipulated in the Rules for Prevention and Control of Coal and Gas Protrusion (8 m^3/t). The results measured in each borehole were analyzed, and we found that the gas content gradually decreases from the outside to the inside of the stop mining line. Therefore, after protective seam exploitation, the overlying coal and surrounding rock mass is sufficiently unpressurized towards the boundary and meets the production requirements.

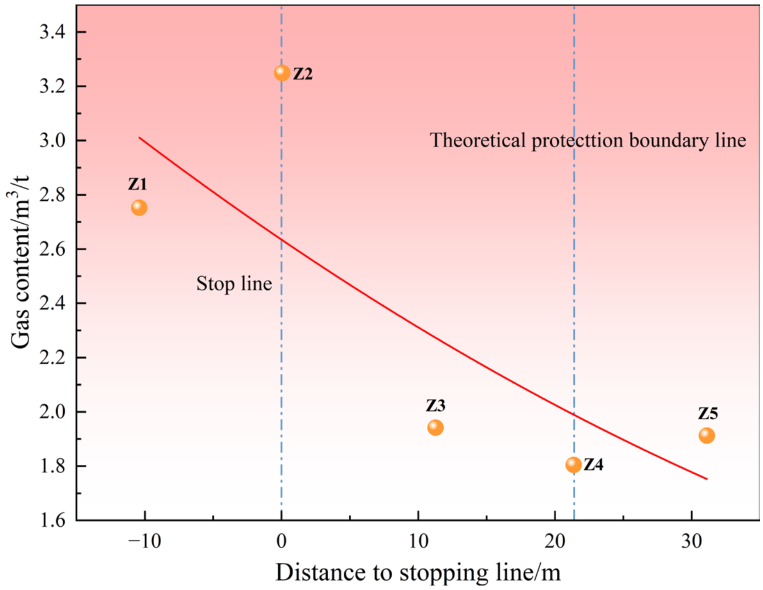

Figure 12. Distribution map of borehole measurement results investigated at strike boundary.

Q1~Q3 boreholes were examined at the inclined upper boundary, and the maximum gas content was determined to be 2.63 m^3/t, as shown in Figure 13. Their values were all less than the critical value for determining the risk of protrusion as stipulated in the Rules for Preventing and Combating Coal and Gas Protrusion (8 m^3/t). As seen from the curves, the gas content shows a non-linear trend of decreasing from the outside of the wind tunnel towards the boundary of the theoretical protection range. The value of residual gas content increases gradually from Q4 to Q7, extending from the theoretical protection boundary line to the outside, with a gradual increase in gas content. Among them, the maximum gas content of 2.35 m^3 was measured in the inspection boreholes, and the gas content of all boreholes was less than the protruding critical value. Pressure unloading of the protected coal seam is sufficient to meet production demand.

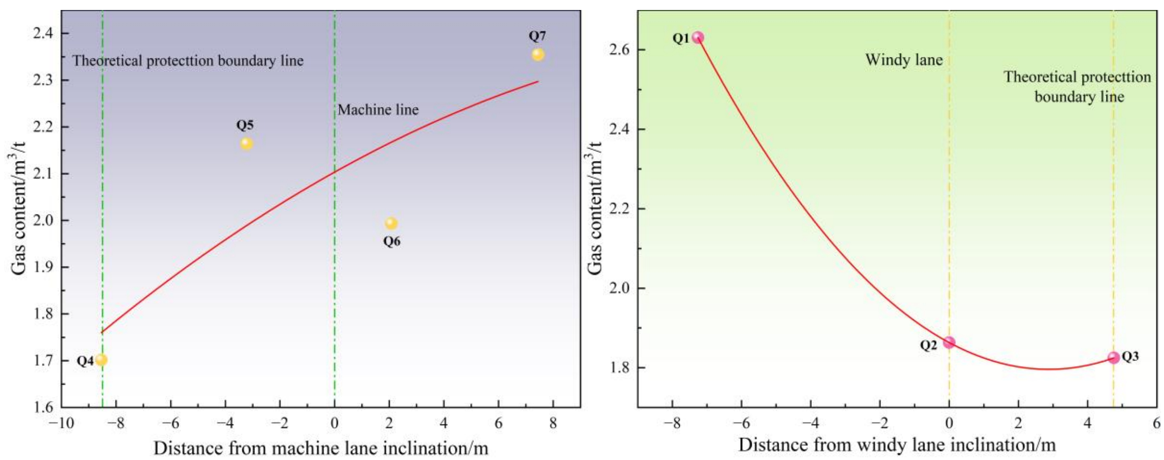

Figure 13. Tendency boundary inspection drill hole measurement distribution map.

5. Conclusions

(1) After protective seam mining, the horizontal stress at the mining boundary of the overlying coal and surrounding rock mass decreased by 88.9% in the strike direction and by 79.7% in the inclination direction, whereas the vertical stress increased by 58.9% and 62.6% in the corresponding directions. This demonstrates a distinct stress evolution pattern at the protected seam boundary, characterized by increased vertical stress and reduced horizontal stress.

(2) Analysis of fracture distribution at the mining boundary of the overlying coal–rock mass shows that, under horizontal stress unloading, a large number of vertical fractures develop along the strike and inclination boundaries of the protected seam. The resulting fracture zone exhibits an inverted trapezoidal geometry, with a wider upper portion and a narrower lower portion.

(3) Based on the permeability–three-dimensional stress evolution model, the permeability at the boundary of the protected coal seam after mining is calculated to increase up to 900 times, with the ratio of post-mining to initial permeability reaching 2.6×10^3. From the center of the seam outward, the permeability distribution of the protected seam can be divided into four zones: a zone of great permeability increase, a zone of permeability increase, a zone of permeability decrease, and a zone of original permeability.

Author Contributions: Conceptualization, J.G., L.W., Z.H., W.Z., Z.Y., H.Z., D.L. and T.W.; Methodology, J.G., L.W., Z.H. and Z.Y.; Software, J.G., L.W., Z.H. and H.Z.; Validation, D.L.; Formal analysis, J.G., Z.H., Z.Y. and H.Z.; Investigation, L.W., W.Z., Z.Y., H.Z., D.L. and T.W.; Resources, H.Z., D.L. and T.W.; Data curation, L.W., Z.H., W.Z., Z.Y. and T.W.; Writing—review & editing, J.G. All authors have read and agreed to the published version of the manuscript.

Funding: The authors are grateful to the National Natural Science Foundation of China (No. 51874298, No. 52174217) and the National Key R&D Program (No. 2022YFC3004702).

Data Availability Statement: The data presented in this study are available on request from the corresponding authors.

Conflicts of Interest: Authors Wei Zhao and Tao Wang were employed by Chensilou Coal Mine, Henan Longyu Energy Co., Ltd. Author Zhengyu Yang was employed by Science and Technology Innovation Center, Henan Energy Group Co., Ltd. Author Dong Liu was employed by Institute of Chemical Engineering and Design, Henan Energy Group Research Institute Ltd. The remaining authors declare that the research was conducted in the absence of any commercial or financial relationships that could be construed as a potential conflict of interest.

References

1. Guo, H.; Yuan, L.; Shen, B.; Qu, Q.; Xue, J. Mining-induced strata stress changes, fractures and gas flow dynamics in multi-seam longwall mining. *Int. J. Rock Mech. Min. Sci.* **2012**, *54*, 129–139. [CrossRef]
2. Zhang, J.; Wang, M.; Wang, Y. Fracture evolution and gas transport laws of coal and rock in one kilometer deep coal mine with complicated conditions. *Therm. Sci.* **2019**, *23*, 907–915. [CrossRef]
3. Zhang, M.; Shimada, H.; Sasaoka, T.; Matsui, K.; Dou, L. Evolution and effect of the stress concentration and rock failure in the deep multi-seam coal mining. *Environ. Earth Sci.* **2013**, *72*, 629–643. [CrossRef]
4. Qin, Y.; Jin, K.; Tian, F.; Su, W.; Ren, S. Effects of ultrathin igneous sill intrusion on the petrology, pore structure and ad/desorption properties of high volatile bituminous coal: Implications for the coal and gas outburst prevention. *Fuel* **2022**, *316*, 123340. [CrossRef]
5. Teng, F.; Yu, M.; Chao, J.; Ma, Z. Coal pillar's breaking and fracture development mechanism and numerical simulation. *Therm. Sci.* **2022**, *26*, 2439–2446. [CrossRef]
6. Zhao, P.; Kang, X.; Li, S.; Lin, H.; Gan, L.; An, X. Optimization of "hole-drift" collaborative drainage layout parameters and high efficient drainage in pressure relief gas migration area. *Coal Sci. Technol.* **2022**, *50*, 137–146.
7. Li, S.; Yang, E.; Lin, H.; Zhao, P. Construction and pratice of accurate gas drainage system for pressure relief gas in deep mining. *Coal Sci. Technol.* **2021**, *49*, 1–10.

8. Chen, S.; Tao, S.; Tang, D. In situ coal permeability and favorable development methods for coalbed methane (CBM) extraction in China: From real data. *Int. J. Coal Geol.* **2024**, *284*, 104472. [CrossRef]
9. Wei, W. Coal Breakage Impact by High Pressure Rotary Water Jet and Induced Pressure Relief and Permeability Enhancement by Hydraulic Flushing Cavity: Mechanism and Application. Doctoral Dissertation, China University of Mining and Technology, Xuzhou, China, 2016.
10. Hu, X.; Sun, Q.; Wang, S.; Wei, S.; Ding, X.; Zhao, X. Study on deterioration characteristics of combustion metamorphic rocks under dry–wet cycling. *Bull. Eng. Geol. Environ.* **2022**, *81*, 467. [CrossRef]
11. Bao, R.; Shi, B.; Zhang, C. Research and Application of "Concentric Ring" Reinforcement and Sealing Technology for Gas Drainage Boreholes in Soft-Coal Seams. *ACS Omega* **2022**, *7*, 34763–34769. [CrossRef]
12. Peng, G.-Y.; Gao, M.-Z.; Xie, J.; Liu, Q.; Deng, G.-D.; Li, C.; He, Z.-Q. Field test research on gas migration law of mining coal and rock. *Therm. Sci.* **2019**, *23*, 1591–1597. [CrossRef]
13. Li, Y.; Zheng, J.; Wang, F.N.; Hu, C.W.; Yang, F.; Ma, X.G.; Tao, Z.G. Movement and deformation characteristics of overlying rock mass in deep coal seam. *J. Mt. Sci.* **2023**, *20*, 1725–1741. [CrossRef]
14. Li, B.; He, Y.; Li, L.; Shi, Z.; Zhang, Y. Damage Characterization and Permeability Variation of Acidified Rock: A Theoretical and Experimental Study. *ACS Earth Space Chem.* **2023**, *7*, 926–935. [CrossRef]
15. Yin, W.; Miao, X.; Zhang, J.; Zhong, S. Mechanical analysis of effective pressure relief protection range of upper protective seam mining. *Int. J. Min. Sci. Technol.* **2017**, *27*, 537–543. [CrossRef]
16. Chen, Y.; Yu, Q. Safe and Efficient Coal and Gas Co-mining System and Application in Coal Seam Groups. *J. China Univ. Min. Technol.* **2003**, *32*, 5–9. [CrossRef]
17. Wang, Z.; Xi, J.; Chen, J.; Li, X.; Li, Y.; Ma, X. Study on time effectiveness of gas drainage by crossing layer drilling in floor rock roadway with one hole and multi-purpose. *Coal Sci. Technol.* **2021**, *49*, 248–256.
18. Xie, J.; Luo, X.; Zhou, Y.; Zhang, J. Numerical Simulation of the Overlying Coal-rock's Deformation Relief Effect During the Protective Layer Mining Process. *Saf. Coal Mines* **2012**, *43*, 163–165.
19. Wei, G. Similarity experiment of rock fracture evolution after covering layer exploitation in hongling coal mine. *J. Liaoning Tech. Univ. (Nat. Sci.)* **2012**, *31*, 185–188.
20. Hao, C. Research on the Mechanism of Quick Stress Relief for Enhancing Permeability by Mechanical Cavitation in Downward Boreholes and Gas Drainage Technology. Doctoral Dissertation, China University of Mining and Technology, Xuzhou, China, 2021.
21. He, Y.; Liu, Y.; Han, H.; Zuo, W.; Chang, P.; Hu, G.; Shi, C. Spatiotemporal evolution model of protected coal seam permeability before and after first fracture of overlying key strata: A case study of Mengjin coal mine. *Environ. Earth Sci.* **2025**, *84*, 557. [CrossRef]
22. Kan, Z.; Zhang, L.; Liu, X.; Wang, C.; Hao, D.; Ye, Z. Coal permeability evolution under coupled mining disturbance and gas extraction conditions: An experimental study. *Nat. Gas Ind. B* **2025**, *12*, 607–622. [CrossRef]
23. Yang, Y.; Jiang, C.; Hou, D.; Yan, F.; Wen, Z. A permeability model considering the dynamic effect of stress on gas adsorption under discontinuous compression. *Sci. Rep.* **2024**, *14*, 24676. [CrossRef]
24. Rong, T.; Yang, H.; Zhang, S.; Ren, X.; Wang, J.; Zhou, Y.; Yang, Y. Permeability evolution of deep coal under the coupling damage of mining-adsorption. *Environ. Earth Sci.* **2025**, *84*, 63. [CrossRef]
25. Zhu, Z.; Xie, J.; Zhang, Y.; Du, Y.; Ren, L.; Ai, T.; Yang, B.; Gao, M. Mining-induced fracture network reconstruction and anisotropic mining-enhanced permeability evaluation using fractal theory. *J. Rock Mech. Geotech. Eng.* **2025**, *17*, 2256–2275. [CrossRef]
26. Perera, M.; Sampath, K. Modelling of free and adsorbed CO_2-induced mechanical property alterations in coal. *Int. J. Coal Geol.* **2020**, *217*, 103348. [CrossRef]
27. Liu, H.; Liu, J.; Zhang, S.; Feng, L.; Qiu, L. Experimental study on compression characteristics of fractured soft rock and its Mohr-Coulomb criterion. *Theor. Appl. Fract. Mech.* **2023**, *125*, 103820. [CrossRef]
28. Xu, C.; Cao, M.; Wang, K.; Fu, Q.; Qin, L. Mining-disturbed coal damage and permeability evolution: Model and validation. *Greenh. Gases Sci. Technol.* **2021**, *11*, 210–221. [CrossRef]
29. Somerton, W.H.; Söylemezoglu, I.M.; Dudley, R.C. Effect of stress on permeability of coal. *Int. J. Rock Mech. Min. Sci. Geomech. Abstr.* **1975**, *12*, 129–145. [CrossRef]